Arab J. Nucl. Sci. Appl., Vol. 56, 4, 27-40 (2023)

ISSN 1110-0451

Arab Journal of Nuclear Sciences and Applications

Web site: ajnsa.journals.ekb.eg

(E S N S A)

Preparation of magnetically separable Fe_3O_4 @ SiO_2@ FeOOH nanoparticles for effective removal of Cr (VI) from aqueous solution

Ahmed M. Soliman *, Ismail M. Ali and Magdy Khalil

Hot Labs. Center, Egyptian Atomic Energy Authority, Egypt

HIGHLIGHTS

1. Selective adsorption of Cr(VI) from solution.
2. Separation of FeOOH loaded with Cr(VI) by magnet.
3. Regeneration of FeOOH using 0.2M NaOH.

GRAPHICAL ABSTRACT

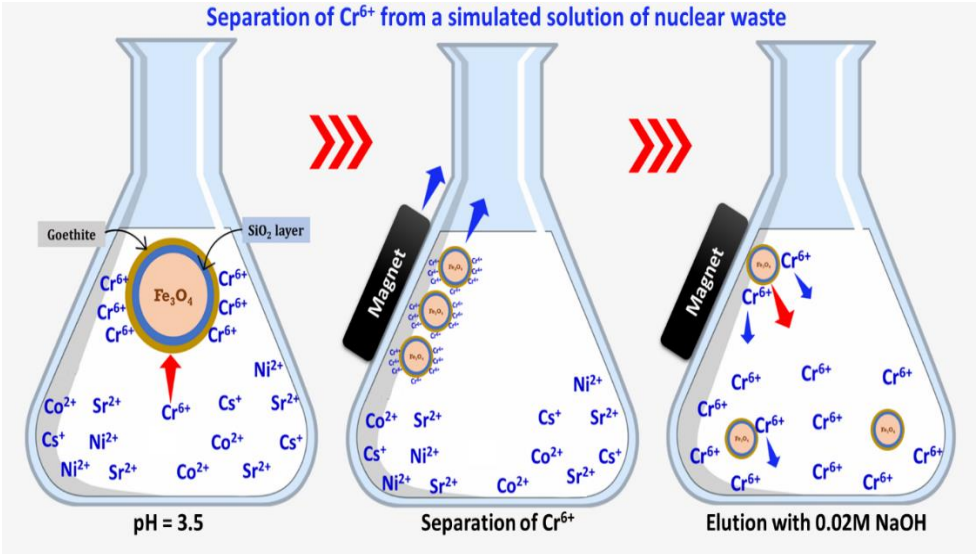

ARTICLE INFO

Article history:

Received: 28th Oct. 2022

Accepted: 7th Dec. 2022

Available online: 6th Mar. 2023

Keywords:

Adsorption;

Chromium;

Goethite;

Silica coated Fe_3O_4;

Aqueous solution treatment.

ABSTRACT

In this study, Fe_3O_4@SiO_2@FeOOH has been prepared and used as an adsorbent to eradicate Cr(VI) from aqueous media. Fe_3O_4@SiO_2@FeOOH has been characterized by various characterization methods. Various factors on chromium adsorption such as the effect of pH, temperature, adsorbent dose, Cr(VI) concentration, and time were studied. The reaction mechanism was determined after applying kinetic models to the adsorption process. It was found that the adsorption amount of Cr(VI) on Fe_3O_4@SiO_2@FeOOH is 42.95 mg/g. The time to reach equilibrium for adsorption is 150 min. Also, the adsorption of Cr(VI) is found to be fitted with pseudo-second order model. The equilibrium studies showed that Cr(VI) is adsorbed according to Langmuir model. As temperature rises, the amount adsorbed is increased. The regeneration and reuse of Fe_3O_4@SiO_2@FeO have been studied for four cycles of Cr(VI) adsorption. 0.2 M NaOH solution is the best eluent of adsorbed Cr(VI) and Fe_3O_4@SiO_2@FeOOH regeneration. It was found that Fe_3O_4@SiO_2@FeOOH can be used efficiently for four cycles.

1. INTRODUCTION

Although chromium (Cr(VI)) is not a by-product of burned nuclear fuel, it is present in high quantities in solutions resulting from the various activities of the nuclear fuel cycle. Chromium salts are added in large quantities as oxidizing and reducing agents in the process of recycling burned nuclear fuel to extract uranium and plutonium. It is also found in radioactive liquid waste from the nuclear fuel cooling cycle as (corrosion products). chromium-nickel alloys are used in nuclear reactors for cladding the fuel rods, as well as for neutron absorbing rods that are used for maintaining reactor safety. The dispersion-type fuel rods for low-power nuclear power plants and floating power units can be coated with chromium-nickel alloy, which also provides the fuel stability needed in emergency

Corresponding author: a.soliman.zidan@gmail.com

DOI: 10.21608/AJNSA.2023.171336.1657

©Scientific Information, Documentation and Publishing Office (SIDPO)-EAEA

situations. Its composition is 42 weight percent chromium, 1.5 weight percent molybdenum, and the rest is nickel [1,2]. Radiation from nuclear accidents and friction of fuel claddings released radioactive chromium ions into the aqueous waste. Generally, Cr(VI) should be separated from cooling water or fission products [3] before discharge or disposal.

For both biotic and abiotic species, Cr is a dangerous heavy metal (with different oxidation states, such as Cr(III), and Cr(VI)). While Cr is present mostly in forms of trivalent (Cr(III)) and hexavalent (Cr(VI)) chromium, the concerns with Cr are primarily related to Cr(VI) owing to its much higher mobility, bioaccumulation, and toxicity [4–6]. It causes cancer in both humans and animals when its concentrations are above 0.05 mg/L. The carcinogenic properties of Cr(VI) are apparent in kidney, liver, and lungs. In water, chromium (Cr(VI)) is highly soluble and forms anions such as chromate (CrO_4^{-2}) and dichromate ($Cr_2O_7^{-1}$) [7].

A variety of methods have been employed to remove Cr(VI), including chemical precipitation [8], electrochemical [9], oxidation/reduction [10], ion exchange [11], membrane [12], ultrafiltration membrane [13], flotation [14], solvent extraction [15], reverse osmosis [16], foam fractionation [17], adsorption and biosorption [18]. Adsorption is an effective and versatile method for removing Cr(VI), particularly when several regeneration steps are included [19]. Adsorption has been regarded as a top technique for eliminating Cr(VI) from waste water because of its exceptional advantages, including ease of handling, high selectivity, economic effectiveness, and environmental friendliness. Many adsorbents, including carbon compounds, metal oxides, and molecular polymers, have been investigated for the removal of Cr(VI) [20–23].

For the elimination of Cr (VI), iron-based compounds have been researched and employed as adsorbents. This is due to the strong magnetic characteristics of iron-based materials and the high level of affinity between chromium and iron, which makes it simple to reuse and separate adsorbents from solutions [24–26]. However, iron oxide nanoparticles alone do not have the advantage of removing Cr(VI) in aqueous systems. Their agglomeration tendency is the biggest challenge due to their magnetic properties. By immobilizing iron oxide nanoparticles into porous media, this drawback can be overcome and the adsorption capacity can be improved [24, 25]. Surface modification of Fe_3O_4 NPs is commonly achieved with silica, a common and widely used agent [29]. As an added benefit, silica coating reduces oxidation, dissolution, and agglomeration of MNPs. So, the stability of MNPs is enhanced [30]. Furthermore, it is simple to regulate the coating-silica layer's size and thickness [31].

The mineral iron oxyhydroxide is found in three chemical formulas, goethite (α-FeOOH), akagoneite (β-FeOOH), and lepidocrocite (γ-FeOOH) [32]. It is one of the most common iron compounds in nature, occurring in many soil types, as well as hematite, kaolinite, and ferrihydrite. As well as sediments and rocks, goethite is present in steel corrosion products. They can absorb cations and anions harmful to human health, such as arsenic, chromium, lead, mercury, selenium, and phosphate [19]. Using goethite in water treatment process has the primary drawback of its segregation at the end of the treatment process since it is a fine powder and thus cannot be recycled or used for column operation. To overcome this drawback, the goethite can be used as a coating on inorganic nano-particles such as silica, sand, or quartz [33–36]. The coating with goethite not only makes the nanoparticles more stable in solution but also provides sites for adsorption. Furthermore, it is simple to regulate the coating-silica layer's size and thickness. The abundance of ironoxy and hydroxyl groups in it also makes it a perfect material for modifications. In accordance with the pH of the solution, these functional groups may allow goethite to remove cationic and anionic species [37].

For the best of our knowledge, removing Cr(VI) from waste water generated from the backend of nuclear fuel cycle activities using Fe_3O_4@SiO_2@FeOOH is not studied. Based on the findings of this study, nano-goethite (FeOOH) was incorporated onto Fe_3O4@SiO_2 to create Fe_3O_4@SiO_2@FeOOH for removing Cr(VI) from aqueous solution. Batch studies were conducted to determine the adsorption capability of Fe_3O_4@SiO_2@FeOOH. The influence of adsorbent dose, time, temperature, pH, and Cr(VI) concentration on adsorption processes was investigated. Also, removal of Cr(VI) from synthetic nuclear waste similar solution was studied. The reusability of the adsorbent was studied as well. The proposed adsorbent was expected to show high selectivity and capacity for removal of Cr(VI) from acidic solution. Simplicity of magnetic separation of the prepared material from the solution at the end of the adsorption process benefits its use for many cycles.

2. MATERIALS AND METHODS

2.1. Materials and instruments

All of the compounds used in this study had a scientific reagent point and were used directly. Tetraethoxysilane, 1,5 – diphenylcarbazide, and Fe_3O_4 nanoparticles (50-100 nm) were purchased from MERCK. Ferrous sulphate and potassium chromate were purchased from Winlab. Ammonium hydroxide and sulfuric acid, $Sr(NO_3)_2$, CsCl, $Co(NO_3)_2$, $Ni(NO_3)_2$ were obtained from Adwick, Egypt. The structure of Fe_3O_4@SiO_2@FeOOH was analyzed by FT-IR spectrophotometer type 540 Thermo Nicolete. Using a scanning electron microscope made by JEOL USA, the morphology of the material surface was investigated. The elemental composition of Fe_3O_4@SiO_2@FeOOH was performed by EDX accompanied with the scanning electron microscope. The surface area for the prepared adsorbent was measured using The Brnauer-Emmett-Teller under nitrogen gas at −196 °C using a physisorption analyzer Micrometrics Tri-Star II plus (Tri-Star II 3020). A muffle furnace CARBOLET, ultrasonic vibration instrumental and an analytical balance of model ADWA, pw124, Germany were used. The equilibrium studies were carried out in a water bath with a thermostat that was designed at Clifton, England. Additionally, pH measurements of various solutions were taken using an Orion 410 A+ pH meter. A Cary-50 UV-Visible spectrophotometer was used to measure the absorbance of the Cr(VI) using 1,5 diphenyl carbazide solutions.

2.2. Silica-coating of iron oxide (Fe_3O_4@SiO_2) nanoparticles

Silica was used to cover the Fe_3O_4 nanoparticles in accordance with previously described procedures. [28,38]. Accordingly, 2 g of Fe_3O_4 powder were uniformly dispersed in 160 mL of ethanol by sonication. After that, 1 mL of tetraethyl orthosilicate (TEOS) and 5 mL of ammonia solution were slowly added to this dispersion, and the mixture was then sonicated for 8 hours. A layer of SiO_2 was directly coated onto the surface of Fe_3O_4 to create (Fe_3O_4@SiO_2). The collected magnetic powder underwent 4 complete washes with distilled water, then the sample was dried at 50 °C. Finally, a permanent magnet was used to create magnetic separation.

Preparation of goethite on the surface of Fe_3O_4@SiO_2 nanoparticles

Goethite was made in accordance with Cheng's instructions [34]. 3.28 g of CH_3COONa and 5.56 g of FeSO4 were dissolved in a 250 mL water after being dissolved in 100 mL of each. Then, a sample of silica-coated iron oxide nanoparticles weighing 1g was added. The mixture was dispersed for 4 hours, in ultrasonic sonication. A permanent magnet was used to create separation. The prepared samples were washed several times with distilled water and then dried for 4 days in an oven at 50 °C.

2.3. Adsorption studies

In order to make a stock solution of 1000 mg/L Cr(VI), 3.2g of K_2CrO_4 was dissolved in distilled water. By dilution, the appropriate concentration of Cr(VI) was prepared using this solution. 25 mL volumetric flasks were used in the batch adsorption experiments that included 10 mg of each of the following: Fe_3O_4, Fe_3O_4@SiO_2, and Fe_3O_4@SiO_2@FeOOH in contact with 10 ml of Cr (VI). To reach equilibrium, the mixture was shaken for 24 hours.

Cr(VI) ion concentration was measured spectrophotometrically [36] as follows:

1 mL of Cr(VI) solution was collected in a 25mL measuring flask. After that 15 mL of 0.1 M HCl was added. Then, 1 mL of 3% 1,5-diphenylcarbazide was added to the mixture. Finally, the mixture was diluted with deionized water to 25 mL and quantified using a spectrophotometer [39].

2.4.1 Effect of adsorbent dose

The influence of the adsorbent dose was investigated. To varied Fe_3O_4@SiO_2@FeOOH masses ranging from 5 to 25 mg at pH 3.5, a volume of 25 mL of Cr(VI) of 100 mg/L was mixed. The equilibrium time was 24 h, and the temperature was 25 °C.

2.4.2 Effect of pH and pH_{pzc}

At an initial ion concentration of 100 mg/L, for 24 h, and 25 °C, the influence of pH on the adsorption of Cr(VI) was examined. 0.1 M of HNO_3 or NaOH was used to modify and adjust the pH value in the range of 1 to 10. The disclosed method was used to determine the pH of the point of zero charge (pHpzc). 20 mL of 0.1M NaCl solution and 50 mg of Fe_3O_4@SiO_2@FeOOH were added to a glass container. In the pH range of 3 to 11, the original pH was measured and modified with 0.1 M HCl or 0.1 M NaOH. For 48 h, the containers were sealed and left. The pH was then measured following the equilibration period. [40,41].

2.4.3 Effect of Cr(VI)concentration and equilibrium studies

10 mg of adsorbent were equilibrated with 25 mL of 100 ppm Cr(VI) solution at 24°C. The pH of the

solution was adjusted at 3.5. At an equilibrium time of 24 h and temperature of 25 ºC, the effect of initial Cr(VI) concentrations was carried at varied values ranging from 50 to 100 mg/L. The final residual concentration of Cr (VI) was determined spectrophotometrically.

2.4.4 Effect of time

The effect of time on the adsorption experiment was studied by equilibrating 20 mg of Fe_3O_4@SiO_2@FeOOH with 50 mL of 100 ppm Cr(VI) at 25º and pH 3.5. 1 mL of Cr(VI) solution at various time intervals were collected and analyzed for Cr(VI) concentration. Using Equations (1) and (2), the % uptake and capacity were calculated.

$$Uptake\,\% = \frac{(C_0 - C_e)}{C_e} x\,100 \qquad (1)$$

$$q_t\,(mg\,/\,g) = \frac{(C_0 - C_e)xV}{m} \qquad (2)$$

Where C_0 and C_e are the initial and equilibrium concentration of ion solution (mg/L) respectively; V is the suspension volume in L, and m is the amount of adsorbent used (g). q_t (mg/g) is the adsorption capacity at different time. All batch adsorption experiments were carried out in triplicate for reproducibility of the data. The obtained experimental data were within the average error limit of 3%.

2.4.5. Effect of temperature

To explore the effect of temperature on the adsorption of Cr(VI) on Fe_3O_4@SiO_2@FeOOH, the adsorption experiments were carried out at three temperatures (280,294, and 308 ºK). 10 mg samples were equilibrated with 25 mL of 100 ppm Cr(VI). The initial pH value was adjusted at 3.5. Also, the adsorption capacity was measured after 150 min.

2.5 Effect of the competing ions

To check its feasibility for application for separation of Cr(VI) from nuclear waste solution generated from spent nuclear fuel reprocessing. An adsorption experiment from a similar nuclear waste solution was carried out. This solution contains different competitive cations and anions. It contains a mixture of 100 mg/L of different cations and oxycations Ni^{+2}, Cs^{+}, Co^{+2}, $Sr^{+2,}$ and ZrO^{+2} . It was prepared by dissolving $Ni(NO_3)_2$, CsCl, $Co(NO_3)_2$, $Sr(NO_3)_2$ and $ZrOCl_2$. $6H_2O$in deionized water. The pH of the produced mixtures was adjusted using 0,1 M HNO_3. The adsorption experiment from this synthetic solution was carried out by equilibration of 20 mg Fe_2O_3@SiO_2@FeOOH with 50 mL of the mixture solution. The concentrations of the cations were measured using ICP-OS Varian spectrophotometer.

3. RESULTS AND DISCUSSION

3.1. Characterisation of the prepared material

3.1.1. SEM and EDX analyses

The SEM image shows homogenous spheres in a porous shape are agglomerated in the range of that 100-250 nm as shown in Fig. 1. The EDX analysis shows the presence of silicon, oxygen, and iron in the prepared compound as shown in Fig. 2 and Table 1. The carbon element appeared from the SEM holder. These results indicate that the FeOOH nanoparticles were successfully loaded on Fe_3O_4@SiO_2.

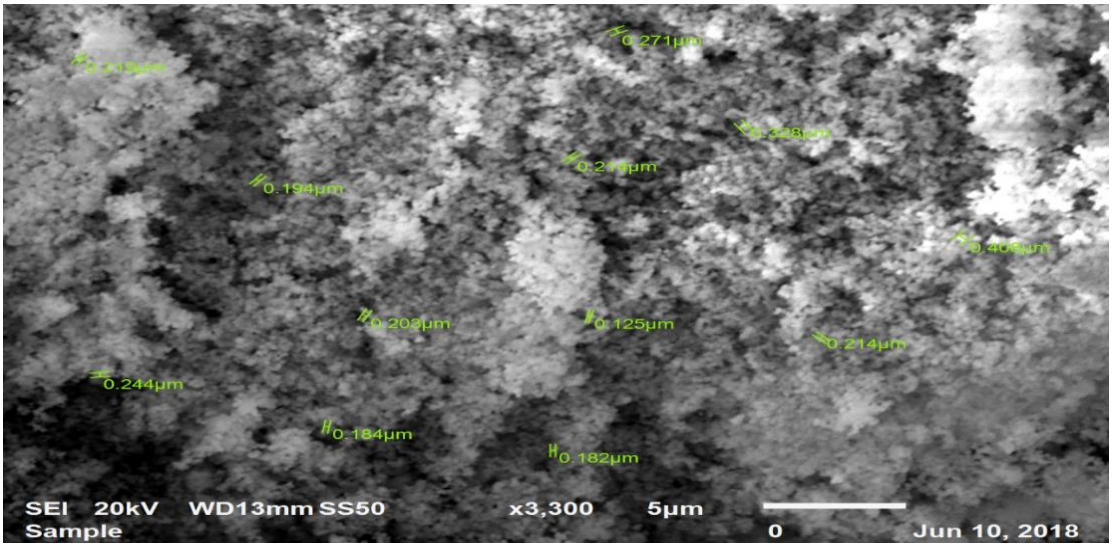

Fig. (1): SEM image of Fe_3O_4@SiO_2@FeOOH.

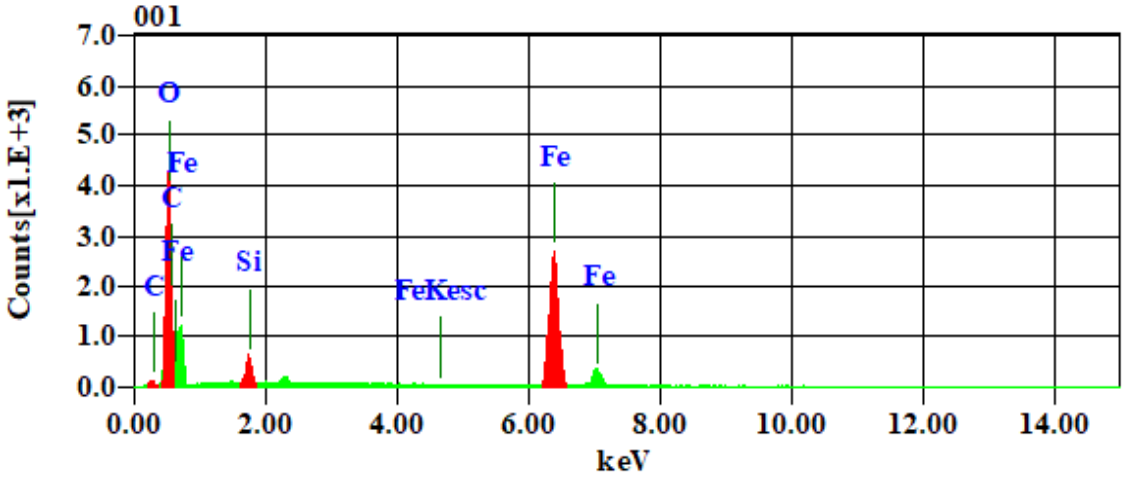

Fig. (2): EDX image of Fe_3O_4@SiO_2@FeOOH.

Table (1): The elemental compositions of Fe_3O_4@SiO_2@FeOOH.

Formula	Mass%	Atom%	Sigma	Net	K ratio Line
C	4.31	9.76	0.03	2574	0.0012662 K
O	34.92	59.03	0.07	110847	0.1851964 K
Si	3.43	3.04	0.04	22137	0.0101503 K
Fe	57.34	28.17	0.14	187726	0.4016782 K
Total	100.00	100.00			

3.1.2. The surface area and IR analysis

The surface area measurements show that the prepared Fe_3O_4@SiO_2 and Fe_3O_4@SiO_2@FeOOH have a surface area of 355 and 390 m^2/g respectively. Also, the coated Fe_3O_4 with SiO_2 kept its mesoporous structure after functionalization with FeOOH. As shown in Fig. 3A.

The FT-IR spectra of Fe_3O_4, Fe_3O_4@SiO_2, and Fe_3O_4@SiO_2@FeOOH are shown in Fig. 3b. A broad peak appeared at ≈3400-3450 cm^{-1} for Fe_3O_4@SiO_2@FeOOH. This peak indicates the presence of OH vibration mode of FeOOH molecule [42,43]. A minor peak which appeared at ≈1650 cm^{-1} for all materials indicate the bending vibration of H-O-H group [44]. A sharp peak which appeared at ≈560 cm^{-1} represents the Fe-O-Si bond (Fig. 3 b and c) [44]. The sharp and duplet wide peak appeared in the range 1100-1200 cm^{-1} in case of each modified product represents the Si-O-Si bond [45]. This reflected the presence of both siloxane and silanol bonds in the silica [43]. The presence of such peaks in case of Fe_3O_4@SiO_2 and Fe_3O_4@SiO_2@FeOOH confirms the successful surface modification of the Fe_3O_4 particles via silica and goethite.

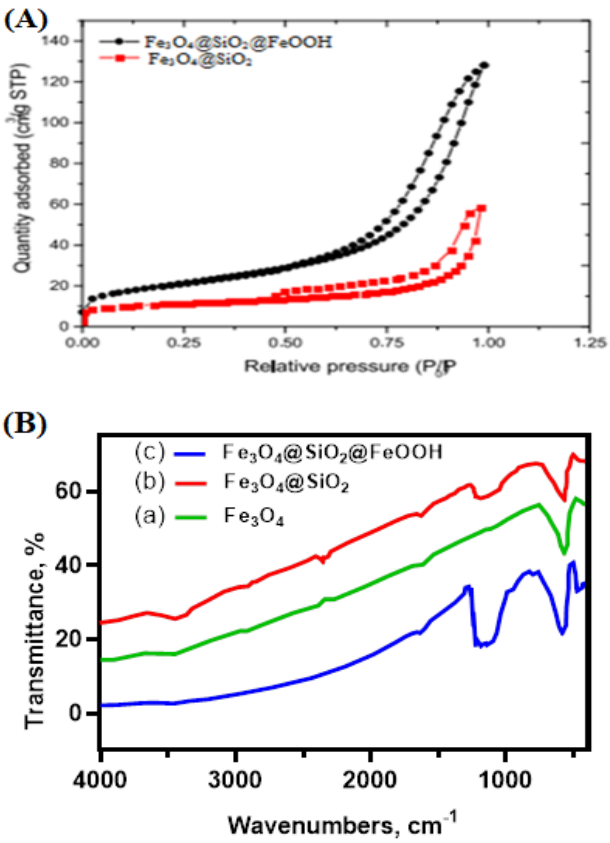

Fig. (3) (A) surface area measurements of Fe_3O_4@SiO_2 and Fe_3O_4@SiO_2@FeOOH. (B) FTIR spectra of (a) Fe_3O_4, (b) Fe_3O_4@SiO_2 and (c) Fe_3O_4@SiO_2@FeOOH.

3.2. Adsorption Studies

Firstly, the adsorption capacity for Cr(VI) was calculated for Fe_3O_4, $Fe_3O_4@SiO_2$, and $Fe_3O_4@SiO_2@FeOOH$ nanoparticles to check the uptake of Cr(IV). The results showed that the obtained capacities are 18, 26, and 45 mg/g for Fe_3O_4, $Fe_3O_4@SiO_2$, and $Fe_3O_4@SiO_2@FeOOH$ respectively. Due to the functionalization with FeOOH, the $Fe_3O_4@SiO_2@FeOOH$ exhibits the maximum adsorption capacity as anticipated.

3.2.1. Effect of adsorbent dose.

The effect of mass of the $Fe_3O_4@SiO_2@FeOOH$ on the adsorption capacity and removal percent of Cr(VI) was also studied. The data are displayed in Fig. 4. It is evident that as the $Fe_3O_4@SiO_2@FeOOH$ dose increased, the adsorption capacity declined[46]. This was expected because with the increasing of adsorbent masses some agglomeration may take place for the nanoparticles which decrease the number of the accessible adsorption sites[47]. However, the findings demonstrate that as the dose of $Fe_3O_4@SiO_2@FeOOH$ was raised, Cr(VI) adsorption uptake also increased. A higher dose of $Fe_3O_4@SiO_2@FeOOH$ results in more active sites and vacancies, enhancing adsorption capacity and removal efficiency.

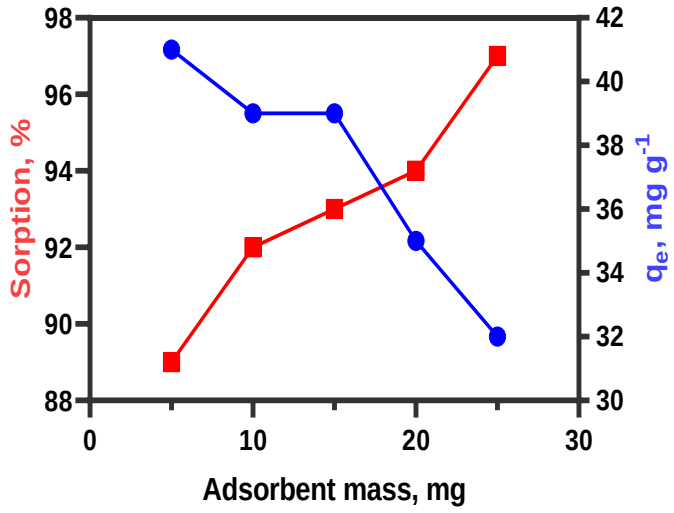

Fig. (4): Effect of $Fe_3O_4@SiO_2@FeOOH$ dose on the adsorption of Cr(VI) (C_0 = 100 mg/L, V=100 ml, pH = 3.5 ± 0.1, time = 24 h, T= 25 °C).

3.2.2. Effect of pH on the adsorption processes and pHpzc

In fact, the pH at the point of zero charge is a very important guideline for the acid-base characteristics of the adsorbents. The plot of the final pH of $Fe_3O_4@SiO_2@FeOOH$ as a function pH is shown in Fig (5 a). This Figure shows that the pHpzc is 5.9. From these results, it can be said that at pH less than 5.9 the surface of $Fe_3O_4@SiO_2@FeOOH$ is positively charged and has a high affinity for the adsorption of negatively adsorbate species. The species of Cr(VI) in the solution are also affected by its pH.

The influence of pH on the adsorption capacity of Cr(VI) was investigated. Fig. 5b depicts the effect of pH change (range of 1 to 10) on the adsorption capacity of $Fe_3O_4@SiO_2@FeOOH$

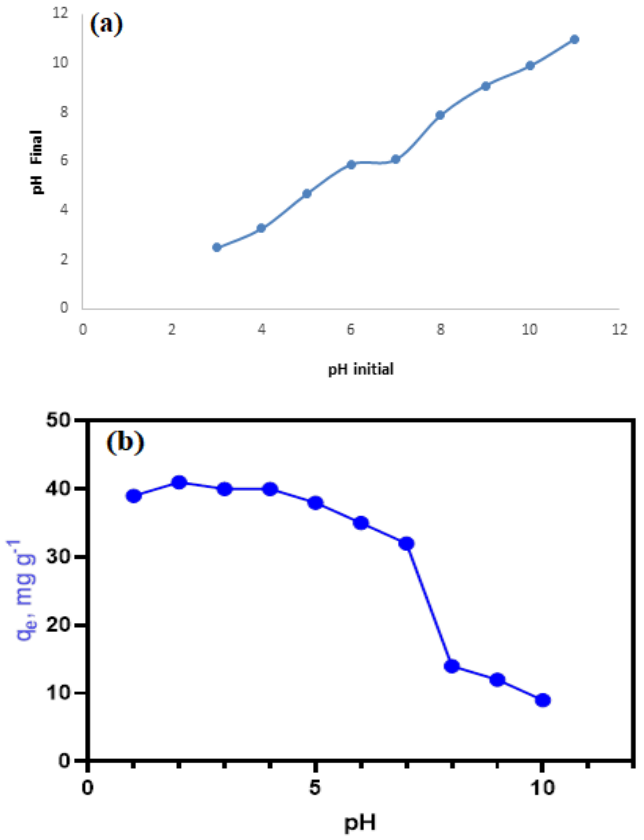

Fig. 5: (a) pH point of zero charge (pHpzc) of $Fe_2O_3@SiO_2@FeOOH$. (b) Effect of pH on the adsorption of Cr(VI) on $Fe_3O_4@SiO_2@FeOOH$ (C_0 = 100 mg/L, m/V=0.2 g/L, time = 24 h, T= 25 °C).

It is clear that the adsorption capacity is high at low pH (less than 5) then it decreases with increasing pH. This finding could be explained as follows: at a lower pH value less than 5.9. $Fe_3O_4@SiO_2@FeOOH$ has a positively charged surface, whereas Cr(VI) occurs as dichromate or chromate, which is a negatively charged species [48]. Therefore, the adsorption capacity increases as a result of the strong electrostatic attraction. At higher pH above 7, the surface of the $Fe_3O_4@SiO_2@FeOOH$ is negatively charged

consequently the electrostatic attraction with negatively charged Cr species is minimal, so the adsorption capacity decreased. Depending on this finding the adsorption of negatively charged Cr(VI) is high in acidic media.. Similar results on the effect of pH were obtained with other adsorbents: activated carbon, silica based and alumina-based adsorbents [49–51].

3.2.3. Effect of Cr (VI) ion concentration

Studying the effect of Cr(VI) ion concentration on both the adsorbent capacity and removal efficiency is significant especially for waste water generated from different industrial activities and its concentration was expected to be high. The percentage removal and adsorption capacity of Cr(VI) are shown in Fig 6. When the initial concentration of Cr(VI) increases, the percent of removal decreases, possibly because every adsorption site on the outside of the adsorbent is filled [52]. On the Fe_3O_4@SiO_2@FeOOH, at low Cr(VI) concentrations there will be a large number of vacant and accessible active binding sites. Because the active sites are blocked, an increase in Cr(VI) concentration inhibits Cr(VI) adsorption. The capacity will increase even if the Cr(VI) concentration increases. Higher initial Cr(VI) concentrations may result in excessive driving forces due to excess mass or chemical potential. At lower concentrations, there is a negligible ratio between free adsorption sites and Cr(VI). As a result, adsorption shifts happen regardless of the initial concentration. Because fewer adsorption sites are accessible as concentrations rise, Cr(VI) removal is influenced by the initial concentration. [53].

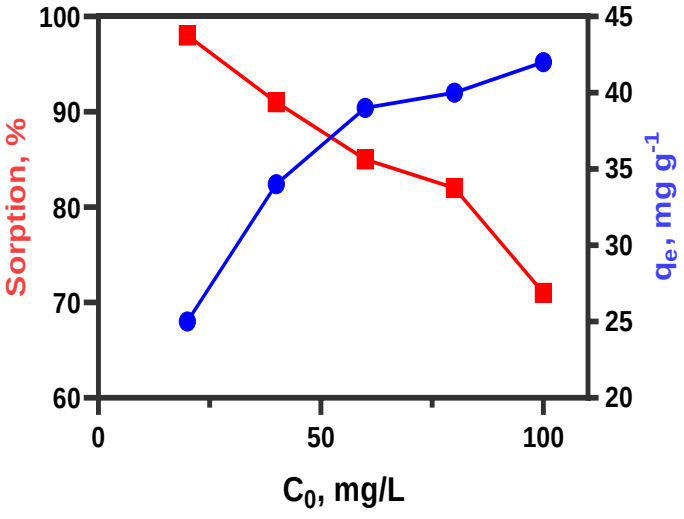

Fig. (6): Effect of initial concentration on the adsorption of Cr(VI) on Fe_3O_4@SiO_2@FeOOH (C_0 = 50 - 100 mg/L, m/V=0.2 g/L, pH = 3.5 ± 0.1, time = 24 h, T= 25 °C).

3.2.4. Effect of contact time

The results of the study on the influence of contact time on Cr(VI) adsorption are shown in Fig. 7. It is evident that the adsorption equilibrium was reached in 100 min with Cr(VI) capacity 47 mgg^{-1}. The material was saturated between 100 and 150 min, indicating no noticeable change in adsorption capacity or percent removal. Therefore, a contact time applied for the batch adsorption experiments is 150 min.

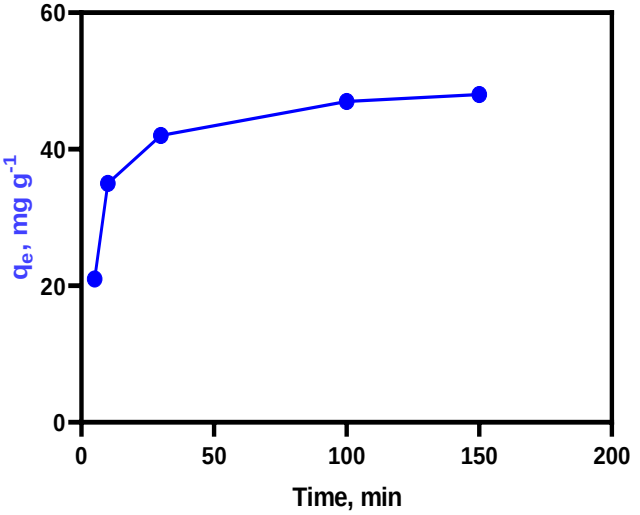

Fig. (7): Effect of contact time on the adsorption of Cr(VI) on Fe_3O_4@SiO_2@FeOOH (C_0 =100 mg/L, m/V=0.2 g/L, pH = 3.5 ± 0.1, T= 25 °C).

3.2.5. Effect of temperature on the adsorption

A study was conducted at three temperatures 280, 294, and 308 °K to determine the effect of temperature on the adsorption capacity of Fe_3O_4@SiO_2@FeOOH for Cr(VI). The adsorption capacity increases with temperature as shown in Fig.8.

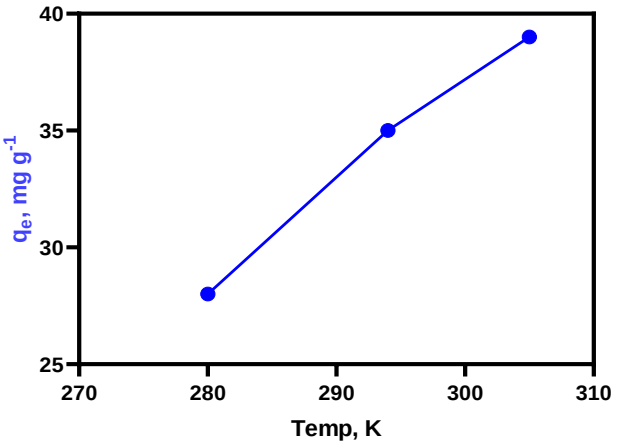

Fig. (8): Effect of reaction temperatures on the adsorption of Cr(VI) on Fe_3O_4@SiO_2@FeOOH (C_0 = 100 mg/L, m/V=0.2 g/L, pH = 3.5 ± 0.1, time = 24 h).

A thermodynamic parameter, including change of enthalpy (ΔH^0), change of entropy (ΔS^0), and Gibbs free energy (ΔG^0), can be determined by the following equations:

$$\ln K_c = -\frac{\Delta H^0}{RT} + \frac{\Delta S^0}{R} \quad (3)$$

$$K_c = \frac{C_0 - C_e}{C_e} \quad (4)$$

$$\Delta G^0 = \Delta H^0 - T\Delta S^0 \quad (5)$$

$$\Delta G^0 = -RT \ln K_c \quad (6)$$

where K_c represents the adsorption equilibrium constant, T (K) is the absolute temperature, and R (8.314 J mol^1 K^1) is the universal gas constant.

Table 2 shows the system's thermodynamic characteristics for adsorption. $\Delta H^0 > 0$ indicated that the adsorption of Cr(VI) on Fe_3O_4@SiO_2@FeOOH is an endothermic process. In addition, $\Delta S^0 > 0$ suggested a disorder in the system, and $\Delta G^0 > 0$ indicated nonspontaneous reactions. Cr(VI) adsorption on Fe_3O_4@SiO_2@FeOOH produced a ΔH^0 value of 14.29 kJ/mol, suggesting that chemisorption was involved. The positive values of ΔS^0 indicate an increasing level of disorder and degree of freedom at the boundary between the adsorbent and the solution during the adsorption process.

Table (2): Thermodynamic parameters for the adsorption of Cr(VI) by Fe_3O_4@SiO_2@FeOOH.

Thermodynamic parameter	ΔG^o, kJ $mole^{-1}$	ΔH^o, kJ $mole^{-1}$	ΔS^o, J $mole^{-1}K^{-1}$
280 (K)	2.12		
294 (K)	1.51	14.29	0.043
305 (K)	1.13		

3.3. Adsorption isotherms

As shown in equations 7 and 8, the Langmuir and Freundlich adsorption isotherm models were applied to investigate further how adsorbents and adsorbates interacted.

$$\frac{C_e}{q_e} = \frac{C_e}{q_{max}} + \frac{1}{q_{max} K_L} \quad (7)$$

$$Ln(q_e) = LnK_f + \frac{1}{n} Ln(C_e) \quad (8)$$

Where q_e (mg/g) and q_{max} (mg/g) indicate the adsorption capacity of Cr(VI) by Fe_3O_4@SiO_2@FeOOH during equilibrium and the maximum adsorption capacity of Fe_3O_4@SiO_2@FeOOH for Cr(VI), respectively; Ce (mg/L) and K_L represent the concentration of Cr(VI) remaining in the adsorption equilibrium solution and the constant of Langmuir equilibrium, respectively. Freundlich constant K_F represents the capacity for adsorption. Freundlich constant n is related to adsorption intensity.

A comparison of the Langmuir and Freundlich models can be found in Fig 9 and Table 3. The fitted adsorption curves are shown in Fig. 9 and the fitting parameters can be found in Table 3. According to the results, Cr(VI) was adsorbable monolayerly on Fe_3O_4@SiO_2@FeOOH surfaces with a R^2>0.999 for the Langmuir model, which indicates that the adsorption occurred on such surfaces. These results were also verified by the above characterization results and the removal test results, that is, the Fe_3O_4@SiO_2 surfaces were uniformly distributed with supported FeOOH particles, and they were complexly adsorbable to Cr(VI) through ironoxy groups. In addition, the fitting results of the Langmuir model (Table 3) showed that the maximum adsorption capacity of Fe_3O_4@SiO_2@FeOOH was 42.95 mg/g.

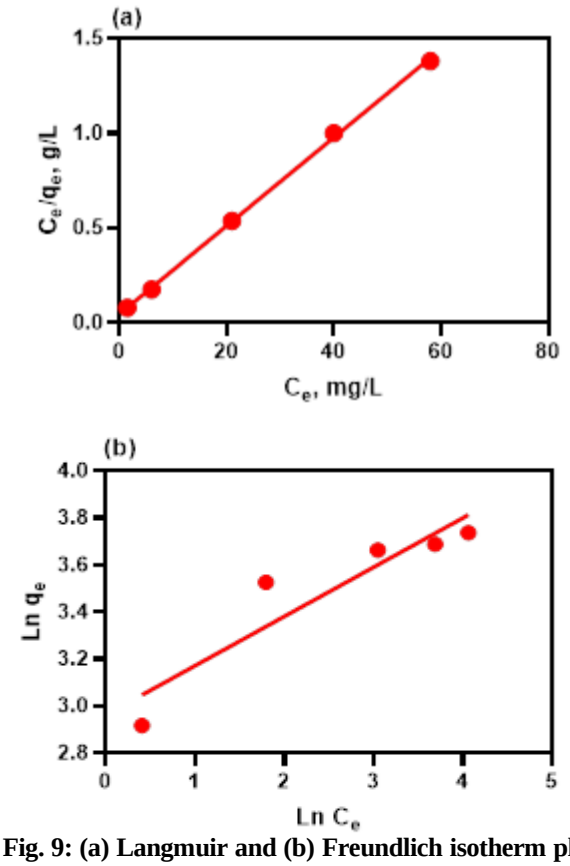

Fig. 9: (a) Langmuir and (b) Freundlich isotherm plots for adsorption of Cr(VI) by Fe_3O_4@SiO_2@FeOOH.

3.4 Adsorption kinetics

Adsorption mechanisms and potential rate-controlling mechanisms (mass transfer, chemical reaction, etc.) were analyzed through kinetic experiments [54,55]. Generally, to evaluate the kinetics of the adsorption process, pseudo-first-order (Eq. (9)) and pseudo-second-order (Eq. (10)) models have been introduced.

$$Ln(q_e - q_t) = Ln(q_e) - K_1 t \quad \textbf{(9)}$$

$$\frac{t}{q_t} = \frac{1}{K_2 q_e^2} + \frac{t}{q_e} \quad \textbf{(10)}$$

Where qe (mg/g) and qt (mg/g) are the adsorption capacity at equilibrium and at a different time. In the pseudo-first-order and pseudo-second-order constant kinetics models, k_1 (min^{-1}) and k_2 (g mg^{-1} min^{-1}) are the rate constants, respectively. The kinetics of Cr(VI) adsorption on $Fe_3O4@SiO_2@FeOOH$ were depicted in Fig. 10 (a and b). Listing the adsorption rate constants derived from adsorption kinetics is given in Table 4.

Table (3): Summarized Langmuir and Freundlich parameters for the adsorption of Cr(VI) by $Fe_3O_4@SiO_2@FeOOH$.

	$Fe_3O_4@SiO_2@FeOOH$
Langmuir isotherm parameters	
q_{max} (mg/g)	42.95
K_L (L/mg)	0.500861
R^2	0.99907
Freundlich isotherm parameters	
n	4.77
K_F ($mg^{n-1}/g.L^n$)	19.35
R^2	0.81326

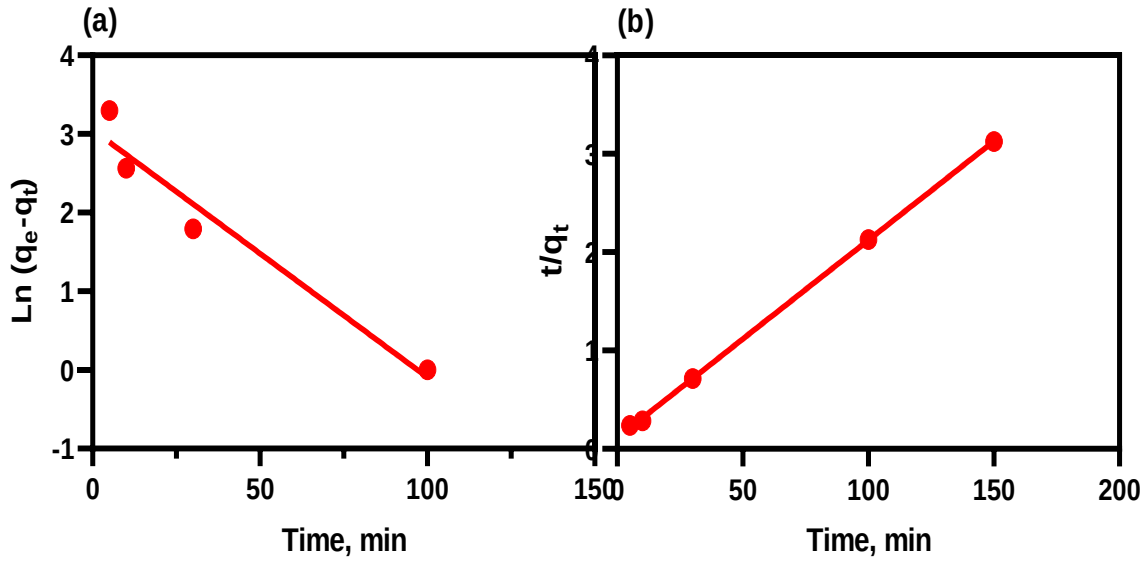

Fig. 10: (a) Pseudo-first-order and (b) pseudo-second-order kinetic models for the adsorption of Cr(VI) by $Fe_3O_4@SiO_2@FeOOH$.

Table (4): Parameters of the pseudo-first-order and pseudo-second-order kinetic models for the adsorption of Cr(VI) by Fe_3O_4@SiO_2@FeOOH.

	Fe_3O_4@SiO_2@FeOOH
Pseudo-first order	
q_e (mg/g) (calculated)	21.195
q_e (mg/g) (experiment)	38.12
K_1 (min^{-1})	0.03147
R^2	0.92524
Pseudo-second order	
q_e (mg/g) (calculated)	49.75
q_e (mg/g) (experiment)	38.12
K_2 (g/mg min)	0.0036
R^2	0.99971

According to Table 4 and Fig. 10 (a and b), the calculated q_e values are in agreement with the theoretical ones, and the plots show a good linearity with R^2 higher than 0.999. Thus, the pseudo-second-order model was more accurately able to describe the adsorption behaviour.

3.5 Effect of different cations

To study the effect of different cations on the adsorption capacity of Cr(VI), similar nuclear waste solution was prepared. Table 5 shows the concentration of different cations, oxycations, and oxyanions before and after mixing with Fe_3O_4@SiO_2@FeOOH tell equilibration. It is clear that a decrease in the concentration of Cr(VI) compared with the other cations The decrease of the concentration of competitive ions is negligible at that pH. However, the calculated adsorption capacity of Fe_3O_4@SiO_2@FeOOH for Cr(VI) is low (32mg/g) in a similar nuclear waste solution compared to 43mg/g in case of pure Cr(VI) solution. This decrease in the adsorption capacity may be attributed to the competitive of other anions present in the solution (as nitrate)for the adsorption sites.

3.6 Comparison with other adsorbents

Comparing Fe_3O_4@SiO_2@FeOOH to other adsorbents for Cr(VI) in the literature is shown in Table 6 [56–61]. It is clear that the Fe_3O_4@SiO_2@FeOOH adsorbent has a large and nearly equal maximum adsorption capacity with Cr(VI), suggesting that this material has a high

Table (5): Effect of different cations on the adsorption of Cr(VI) by Fe_3O_4@SiO_2@FeOOH.

Cations	Conc. before adsorption (mg/L)	Conc. after adsorption (mg/L)
Co(II)	95	93
Ni(II)	99	98
Sr(II)	92	90
Cs(I)	90	91
ZrO (II)	98	97
Cr(VI)	99	71

Table (6): Adsorption capacities of different adsorbents from the literature for the removal of Cr(VI).

Adsorbent	Time, min	Initial pH	Initial Concentration mgL^{-1}	Adsorption capacity (mgg^{-1})	Reference
Graphite/LDHs	300	7.0	20	13.44	[54]
Fe_3O_4@SiO_2@MgAl-borate LDH	240	5.3	30	86.73	[55]
3D hierarchical GO-NiFe	350	6	100	53.6	[56]
Polypyrrole-Modified LDHs	100	5	50	76.21	[57]
MoS_2 coated MgAl composites	100	5. 0	50	76.3	[58]
Arginine-functionalized polyaniline@ FeOOH	420	2.0	700	682.3	[59]
Fe_3O_4@SiO_2@FeOOH	180	4.5	100	42.95	This work

adsorption efficiency and can be a highly effective adsorbent material for removing Cr(VI) from wastewater.

3.6 Regeneration and reusability of the adsorbent.

Regeneration and reusability of the adsorbent is important for the adsorbent and adsorbate as in Fig. 11. The Fe_3O_4@SiO_2@FeOOH loaded with Cr(VI) was separated with a magnet then washed with deionized water and dried at 60ºC. Different concentrations of hydrochloric acid and sodium hydroxide were used for the resorption of Cr(VI).

$$E\ (\%) = \frac{C_1 V_1}{m_1} 100 \qquad (11)$$

Where C_1 (mg/L) is the concentration of the eluent, V_1 (L) is the volume of the eluent, and m_1 (mg) is the mass of the adsorbed solute on the Fe_3O_4@SiO_2@FeOOH.

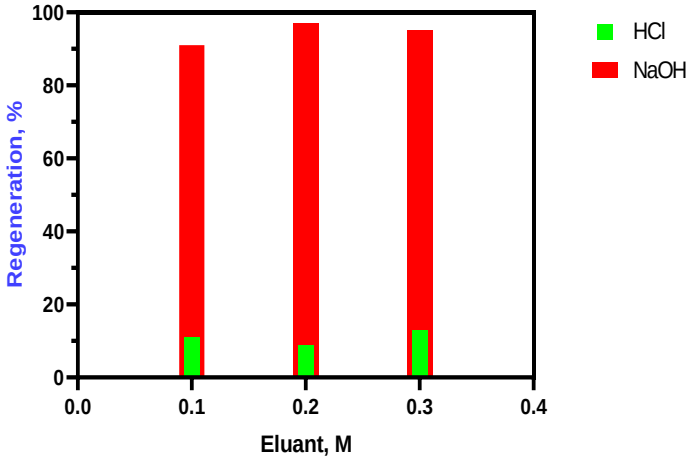

Fig. (11): Regeneration of Cr(VI) on Fe_3O_4@SiO_2@FeOOH using different reagents.

The elution efficiency (E%) of regeneration was calculated as follows.

The highest efficiency of regeneration was found with 0.2 M NaOH. The prepared Fe_3O_4@SiO_2@FeOOH was tested for four cycles of adsorption and resorption by 0.2 M NaOH. Fig. 12 shows the result of recycling. It is clear that the prepared adsorbent could be used efficiently for removing Cr(VI) from water for four consecutive cycles.

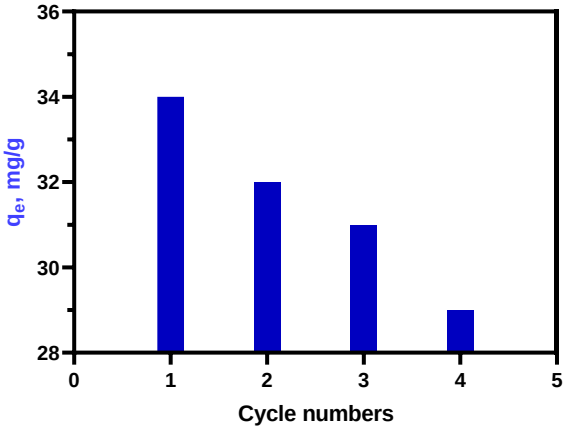

Fig. (12): The adsorption capacity after three cycles of Cr(VI) on Fe_3O_4@SiO_2@FeOOH.

3.7 Adsorption mechanism

FeOOH particles significantly enhance the surface area of Fe_3O_4@SiO_2 and provide more adsorption sites due to their positively charged surfaces and iron-oxyhydroxy groups [62]. Cr(VI) ions may also be adsorbed by coordination interactions as shown by Schem1. It appears that chemisorption was the main controlling process, as the calculated adsorption enthalpy change was positive, and the adsorption increased with increasing temperatures.

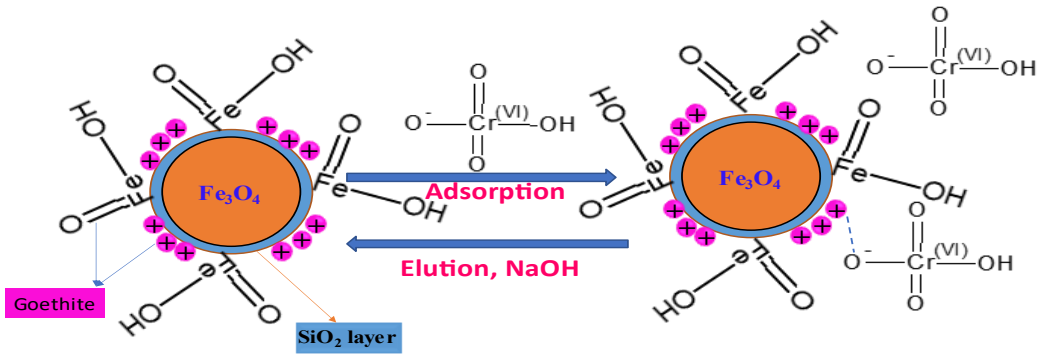

Scheme (1): Schematic diagram of the adsorption and regeneration processes of Cr(VI) by Fe_3O_4@SiO_2@FeOOH.

4. CONCLUSION

Fe_3O_4@SiO_2@FeOOH has been successfully prepared and has shown high efficiency in removing Cr(VI) from aqueous solutions. The highest removal rate for Cr(VI) was achieved at pH 3.5. Adsorption equilibrium of Cr(VI) was reached after 150 min. Fe_3O_4@SiO_2@FeOOH exhibited an adsorption capacity of 47 mg/g and was highly dependent on the Cr(VI) ion concentration, temperature, and reaction time. A low concentration of Cr(VI) was obtained with high adsorption efficiency and fast kinetics using Fe_3O_4@SiO_2@FeOOH, which was well fitted to pseudo-second order and Langmuir equations. The 0.2 M NaOH was found to be the best eluent for the regeneration and reuse of Fe_3O_4@SiO_2@FeOOH for four cycles. As a result of the parameters studied, Fe_3O_4@SiO_2@FeOOH can adsorb Cr(VI) efficiently from the solution. The prepared adsorbent could be applied for the separation of Cr(VI) from acidic solution as waste water generated from nuclear and leather industries. However, more studies are needed to increase the stability of the adsorbent against the corrosion and oxidation of the magnetic nanoparticles.

ACKNOWLEDGMENTS

The authors thank all the staff members and colleagues of the Nuclear Fuel Technology Department, Hot Laboratories Centre of Egyptian Atomic Energy Authority for their cooperation, and useful help offered during this work.

ETHICAL APPROVAL

Not applicable.

CONSENT TO PARTICIPATE

Not applicable.

CONSENT TO PUBLISH

Not applicable.

AUTHORS CONTRIBUTIONS

All authors contributed to the study conception and design. Material preparation, data collection and analysis were performed by [***Prof. Dr. Ahmed M. Soliman***], [***. Dr. Ahmed M. Soliman***] and [***Assoc. Prof. M. Khalil***]. The first draft of the manuscript was written by [***Dr. Ahmed M. Soliman***]] and all authors commented on previous versions of the manuscript. All authors read and approved the final manuscript.

FUNDING

The authors declare that no funds, grants, or other support were received during the preparation of this manuscript.

AVAILABILITY OF DATA AND MATERIALS

Available

COMPETING INTERESTS

The authors declare no competing interests.

REFERENCES.

[1] G. V. Kulakov, A. V. Vatulin, S. A. Ershov, L. A. Karpyuk, Y. V. Konovalov, A. O. Kosaurov, M. V. Leontyeva-Smirnova, V. N. Rechitsky, and A. A. Golubnichy, At. Energy **130**, 25 (2021).

[2] D. Diniasi, F. Golgovici, A. Anghel, M. Fulger, C. C. Surdu-Bob, and I. Demetrescu, Coatings **11**, (2021).

[3] N. C. Division and N. Science, **22**, 143 (1975).

[4] Y. Cong, L. Shen, B. Wang, J. Cao, Z. Pan, Z. Wang, K. Wang, Q. Li, and X. Li, Water Res. **222**, 118919 (2022).

[5] Y. Wang, Y. Gong, N. Lin, L. Yu, B. Du, and X. Zhang, J. Colloid Interface Sci. **606**, 941 (2022).

[6] S. A. Tandekar, M. A. Pande, A. Shekhawat, E. Fosso-Kankeu, S. Pandey, and R. M. Jugade, Minerals **12**, 874 (2022).

[7] M. O. Borna, M. Pirsaheb, M. V. Niri, R. K. Mashizie, B. Kakavandi, M. R. Zare, and A. Asadi, J. Taiwan Inst. Chem. Eng. **68**, 80 (2016).

[8] B. Xie, C. Shan, Z. Xu, X. Li, X. Zhang, J. Chen, and B. Pan, Chem. Eng. J. **308**, 791 (2017).

[9] F. Yao, M. Jia, Q. Yang, K. Luo, F. Chen, Y. Zhong, L. He, Z. Pi, K. Hou, and D. Wang, Chemosphere **260**, 127537 (2020).

[10] B. A. Marinho, R. O. Cristóvão, R. A. R. Boaventura, and V. J. P. Vilar, Environ. Sci. Pollut. Res. **26**, 2203 (2019).

[11] Y. Xie, J. Lin, J. Liang, M. Li, Y. Fu, H. Wang, S. Tu, and J. Li, Chem. Eng. J. **378**, 122107 (2019).

[12] F. Sellami, O. Kebiche-Senhadji, S. Marais, L. Colasse, and K. Fatyeyeva, Sep. Purif. Technol. **248**, 117038 (2020).

[13] Y. Zhang, X. Xu, C. Yue, L. Song, Y. Lv, F. Liu, and A. Li, Chem. Eng. J. **404**, 126546 (2021).

[14] H. Zheng, S. Zhang, C. Yang, H. Yin, W. Liu, and K. Lu, J. Mol. Liq. **342**, 117551 (2021).

[15] P. K. Saw, A. K. Prajapati, and M. K. Mondal, J. Mol. Liq. **269**, 101 (2018).

[16] I. Shigidi, A. E. Anqi, A. Elkhaleefa, A. Mohamed, I. H. Ali, and E. I. Brima, Water **14**, 44 (2021).

[17] J. Lu, Z. Liu, Z. Wu, W. Liu, and C. Yang, Sep. Purif. Technol. **237**, 116346 (2020).

[18] S. K. Gunatilake, Methods **1**, 14 (2015).

[19] G. A. Waychunas, C. S. Kim, and J. F. Banfield, J. Nanoparticle Res. **7**, 409 (2005).

[20] H. Liang, B. Song, P. Peng, G. Jiao, X. Yan, and D. She, Chem. Eng. J. **367**, 9 (2019).

[21] M. Bhaumik, A. Maity, V. V Srinivasu, and M. S. Onyango, J. Hazard. Mater. **190**, 381 (2011).

[22] V.-P. Dinh, M.-D. Nguyen, Q. H. Nguyen, T.-T. Luu, A. T. Luu, T. D. Tap, T.-H. Ho, T. P. Phan, T. D. Nguyen, and L. V Tan, Chemosphere **257**, 127147 (2020).

[23] W. Zhang, S. Zhang, J. Wang, M. Wang, Q. He, J. Song, H. Wang, and J. Zhou, Chemosphere **203**, 188 (2018).

[24] M. Khalil, Y. F. El-Aryan, and I. M. Ali, J. Inorg. Organomet. Polym. Mater. **26**, (2016).

[25] Y. Fang, X. Wu, M. Dai, A. Lopez-Valdivieso, S. Raza, I. Ali, C. Peng, J. Li, and I. Naz, J. Clean. Prod. **312**, 127678 (2021).

[26] Y. Yi, G. Tu, P. E. Tsang, S. Xiao, and Z. Fang, Mater. Lett. **234**, 388 (2019).

[27] N. Zhu, H. Ji, P. Yu, J. Niu, M. U. Farooq, M. W. Akram, I. O. Udego, H. Li, and X. Niu, Nanomaterials **8**, 810 (2018).

[28] M. Namdeo, Adv. Recycl. Waste Manag. **2**, 1000135 (2018).

[29] T. Saragi, H. D. Sinaga, F. Rahmi, G. A. Pramesti, A. Sugiarto, A. Therigan, B. Permana, and N. Syakir, in *Key Eng. Mater.* (Trans Tech Publ, 2020), pp. 83–88.

[30] L. Liu, L. Zhao, J. Liu, Z. Yang, G. Su, H. Song, J. Xue, and A. Tang, J. Mol. Liq. **299**, 112222 (2020).

[31] Z. Sharafi, B. Bakhshi, J. Javidi, and S. Adrangi, Iran. J. Pharm. Res. IJPR **17**, 386 (2018).

[32] R. Chitrakar, S. Tezuka, A. Sonoda, K. Sakane, K. Ooi, and T. Hirotsu, J. Colloid Interface Sci. **298**, 602 (2006).

[33] X. Zhang, H. Niu, J. Yan, and Y. Cai, Colloids Surfaces A Physicochem. Eng. Asp. **375**, 186 (2011).

[34] T. Cheng, M. O. Barnett, E. E. Roden, and J. Zhuang, Environ. Sci. Technol. **38**, 6059 (2004).

[35] C. Xu, D. Cheng, B. Gao, Z. Yin, Q. Yue, and X. Zhao, Front. Environ. Sci. Eng. **6**, 455 (2012).

[36] C. Xu, J. Shi, W. Zhou, B. Gao, Q. Yue, and X. Wang, Chem. Eng. J. **187**, 63 (2012).

[37] J. Han and L. E. Katz, Geochim. Cosmochim. Acta **244**, 248 (2019).

[38] C. Hui, C. Shen, J. Tian, L. Bao, H. Ding, C. Li, Y. Tian, X. Shi, and H.-J. Gao, Nanoscale **3**, 701 (2011).

[39] S. Balasubramanian and V. Pugalenthi, Talanta **50**, 457 (1999).

[40] N. J. Ndi, M. J. Ketcha, G. S. Anagho, N. J. Ghogomu, and E. P. Belibi, Int. J. Adv. Chem. Technol. **3**, 1 (2014).

[41] N. Y. Rachel, N. J. Nsami, B. B. Placide, K. Daouda, A. A. Victoire, T. M. Benadette, and K. J. Mbadcam, Int. J. Innov. Sci. Eng. Technol **2**, 606 (2015).

[42] A. M. Soliman, H. A. Madbouly, E. S. El Sheikh, M. Khalil, and A. Massad, J. Radioanal. Nucl. Chem. **330**, 207 (2021).

[43] A. S. Dewanto, D. H. Kusumawati, N. P. Putri, A. Yulianingsih, I. K. F. Sa'adah, A. Taufiq, N. Hidayat, S. Sunaryono, and Z. A. I. Supardi, in *IOP Conf. Ser. Mater. Sci. Eng.* (IOP Publishing, 2018), p. 12010.

[44] H. Shao, J. Qi, T. Lin, and Y. Zhou, Ceram. Int. **44**, 2255 (2018).

[45] I. Ali, E. Zakaria, S. Shama, and I. El-Naggar, J. Radioanal. Nucl. Chem. **285**, 239 (2010).

[46] M. Khalil, M. M. Shehata, O. Ghazy, S. A. Waly, and Z. I. Ali, Radiat. Phys. Chem. **190**, 109811 (2022).

[47] M. Khalil, H. A. Madbouly, E. M. A. Elgoud, and I. M. Ali, J. Inorg. Organomet. Polym. Mater. (2022).

[48] C. Cui, Y.-D. Xie, J.-J. Niu, H.-L. Hu, and S. Lin, J. Inorg. Organomet. Polym. Mater. **32**, 840 (2022).

[49] F. Gorzin and M. M. Bahri Rasht Abadi, Adsorpt. Sci. Technol. **36**, 149 (2018).

[50] J. Qiu, Z. Wang, H. Li, L. Xu, J. Peng, M. Zhai, C. Yang, J. Li, and G. Wei, J. Hazard. Mater. **166**, 270 (2009).

[51] N. R. Bishnoi, M. Bajaj, and N. Sharma, Environ. Technol. **25**, 899 (2004).

[52] L. J. Yu, S. S. Shukla, K. L. Dorris, A. Shukla, and J. L. Margrave, J. Hazard. Mater. **100**, 53 (2003).

[53] O. Abuzalat, D. Wong, and M. A. Elsayed, J. Inorg. Organomet. Polym. Mater. **32**, 1924 (2022).

[54] I. M. Ali, E. S. Zakaria, M. Khalil, A. El-tantawy, and F. A. El-Saied, J. Inorg. Organomet. Polym. Mater. **30**, 1537 (2020).

[55] M. Khalil, T. Y. Mohamed, and A. El-tantawy, J. Inorg. Organomet. Polym. Mater. **27**, 757 (2017).

[56] Z. Hu, L. Cai, J. Liang, X. Guo, W. Li, and Z. Huang, J. Clean. Prod. **209**, 1216 (2019).

[57] J. Miao, X. Zhao, Y.-X. Zhang, and Z.-H. Liu, J. Alloys Compd. **861**, 157974 (2021).

[58] Y. Zheng, B. Cheng, W. You, J. Yu, and W. Ho, J. Hazard. Mater. **369**, 214 (2019).

[59] S. Sahu, P. Kar, N. Bishoyi, L. Mallik, and R. K. Patel, J. Chem. Eng. Data **64**, 4357 (2019).

[60] J. Wang, P. Wang, H. Wang, J. Dong, W. Chen, X. Wang, S. Wang, T. Hayat, A. Alsaedi, and X. Wang, ACS Sustain. Chem. Eng. **5**, 7165 (2017).

[61] A. Hsini, M. Benafqir, Y. Naciri, M. Laabd, A. Bouziani, M. Ez-zahery, R. Lakhmiri, N. El Alem, and A. Albourine, Colloids Surfaces A Physicochem. Eng. Asp. **617**, 126274 (2021).

[62] B. Zhang, Y. Wu, and Y. Fan, J. Inorg. Organomet. Polym. Mater. **29**, 290 (2019).